Supplementary Information of

Structural, vibrational and electronic properties of α'-Ga_2S_3 under compression

S. Gallego-Parra[1]*, R. Vilaplana[2]*, O. Gomis[2], E. Lora da Silva[1,3], A. Otero-de-la-Roza[4], P. Rodríguez-Hernández[5], A. Muñoz[5], J. González[6], J.A. Sans[1], V.P. Cuenca-Gotor[1], J. Ibáñez[7], C. Popescu[8] and F. J. Manjón[1]

[1]*Instituto de Diseño para la Fabricación y Producción Automatizada, MALTA Consolider Team, Universitat Politècnica de València, 46022 València, Spain*
[2] *Centro de Tecnologías Físicas, MALTA Consolider Team, Universitat Politècnica de València, 46022 Valencia, Spain*
[3]*IFIMUP, Department of Physics and Astronomy, Faculty of Science, University of Porto, Portugal*
[4]*Departamento de Química Física y Analítica, MALTA Consolider Team, Facultad de Química, Universidad de Oviedo, 33006 Oviedo, Spain*
[5]*Departamento de Física, Instituto de Materiales y Nanotecnología, MALTA Consolider Team, Universidad de La Laguna, 38207 San Cristóbal de La Laguna, Spain*
[6]*Ciencias de la Tierra y Fisica de la Materia Condensada, MALTA Consolider Team, Universidad de Cantabria, 39005, Santander, Spain*
[7] *Institute of Earth Sciences Jaume Almera, MALTA Consolider Team, Consell Superior d'Investigacions Científiques (CSIC), 08028 Barcelona, Catalonia, Spain*
[8]*ALBA-CELLS, MALTA Consolider Team,08290 Cerdanyola del Valles (Barcelona), Catalonia, Spain*

*Corresponding author: S. Gallego-Parra (sagalpar@doctor.upv.es), R. Vilaplana (rovilap@fis.upv.es)

Structural properties

Alfa Aesar product specification certifies the existence of a small amount of oxide, Ga_2O_3, in the commercial powders of Ga_2S_3. At room conditions, Ga_2O_3 exhibits a monoclinic β phase (S.G. C2/m, No 12). By means of Le Bail refinements, we have succeeded in indexing α'-Ga_2S_3 together with β-Ga_2O_3 in our XRD pattern at 0.1 GPa, as depicted in **Fig. S1**. Those peaks coming from the β-Ga_2O_3 are located at around 8.20, 8.30, 9.10, 9.50, 10.13 and 12.30 degrees. It is worthy to stress the high intensity of the diffraction peaks from β-Ga_2O_3 at 8.20, 8.30 and 9.50 degrees. The high structure factor values of these peaks explain these high intensities, even at the very low concentration in our commercial powders of Ga_2S_3.

According the Lai et al.'s patterns,[1] they found peaks associated with the impurity, concretely, at 0.39 $Å^{-1}$ in Run-1 (0.0001 GPa, **Fig. 1** of **Ref. 1**) and additionally other peak at 0.3 $Å^{-1}$ in Run-2 (0.1 GPa, **Fig. 2** of **Ref. 1**). Since the limited number of peaks, they could not identify such an impurity. In our HP-XRD conditions, these peaks must be located at 7.30 and 9.5 degrees. That peak observed at 9.5 degrees corresponds with the most intense peak observed of β-Ga_2O_3 in our measurement at 0.1 GPa (**Fig. S1**). However, we have not observed the peak at 7.30 degrees. Therefore, this must correspond to other impurity different from β-Ga_2O_3. To avoid confusion, henceforth we will refer to the β-Ga_2O_3 as the only impurity in our work.

Figure S1. Experimental powder XRD pattern (open circles) of α'-Ga_2S_3 measured at 0.1 GPa. Le Bail refinement (red line) with the used background (green line) and residuals (black line) are also shown. Tick marks correspond to α'-Ga_2S_3, β-Ga_2O_3 and Cu reflections, respectively. Asterisks indicate those diffraction peaks observed from the β-Ga_2O_3.

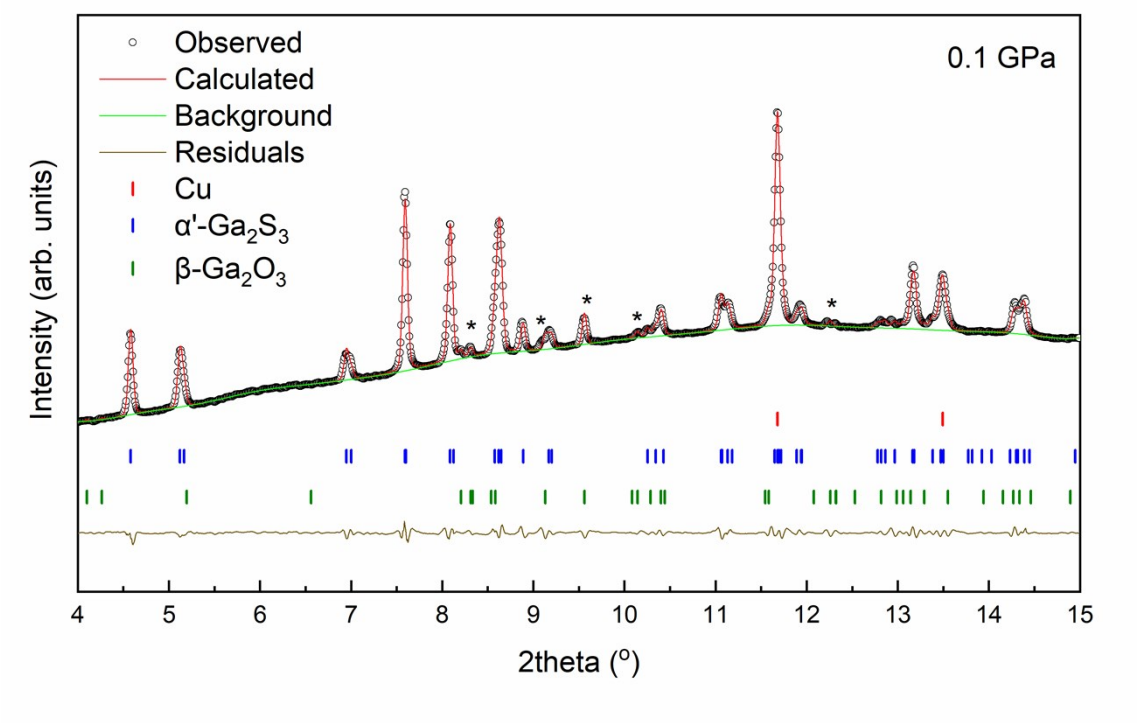

Figure S2. Normalized stress, F_E, vs finite strain, f_E, for a) our experimental data and b) experimental data from run-2 in **Ref. 1**, c) our GGA-PBEsol calculations and d) LDA calculations from **Ref. 1** for the α' phase. Horizontal dash lines serve as a reference of $B_o^{'}$ = 4.

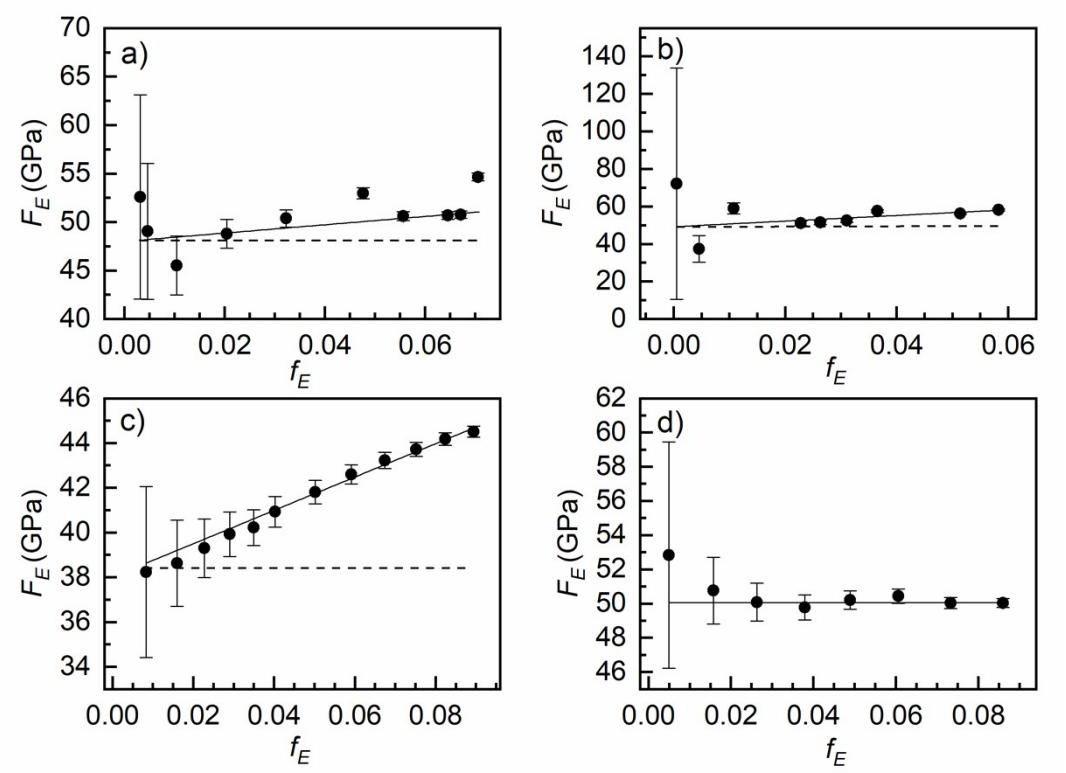

Figure S3. Pressure dependence of the relative volumes in α'-Ga_2S_3 corresponding to the unit-cell and to the $Ga1S_4$ and $Ga2S_4$ tetrahedra.

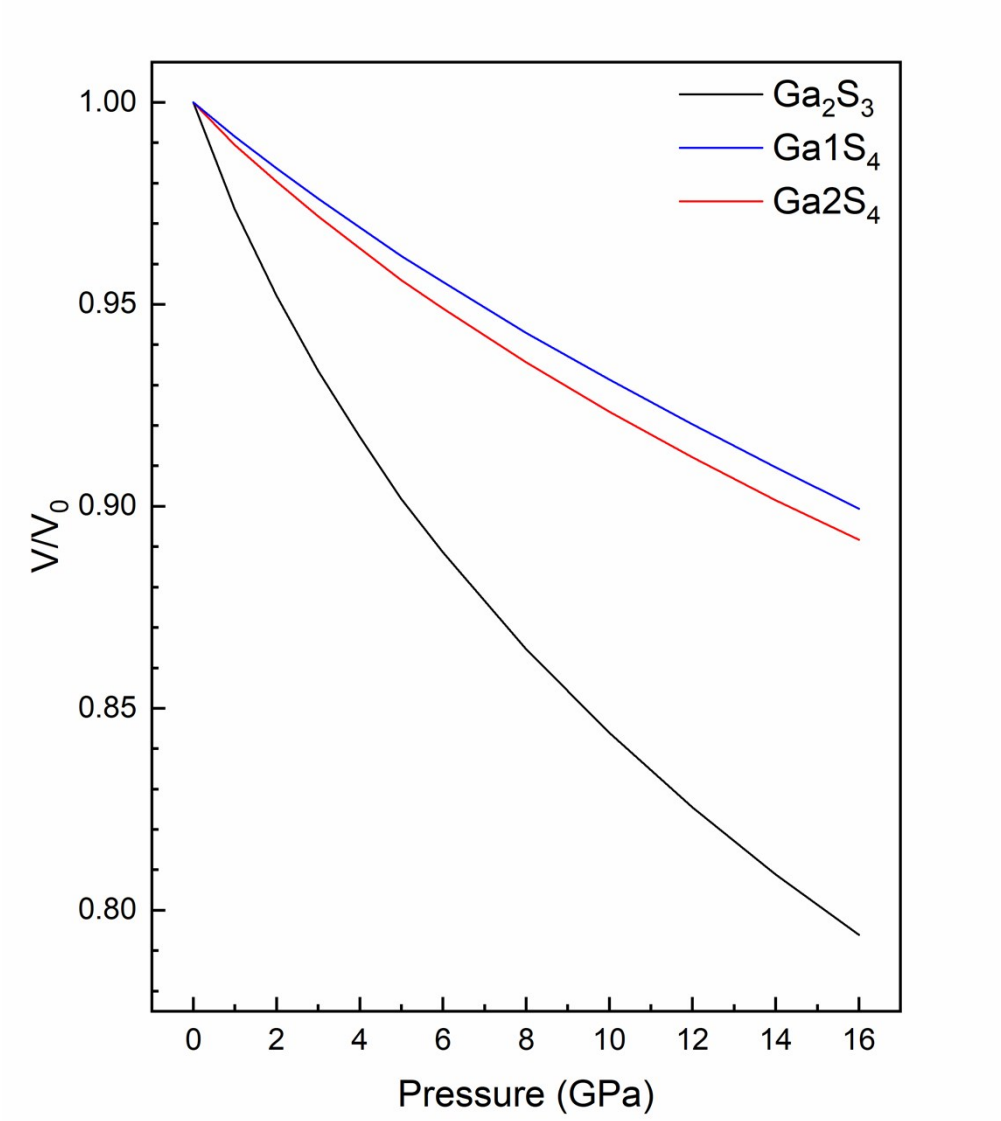

Figure S4. Pressure dependence of the a) ECoN and distortion index and b) bond angle variance and quadratic elongation in $Ga1S_4$ and $Ga2S_4$ polyhedra. Inset on b) depicts the Ga2 atom out the centroid of the $Ga2S_4$ tetrahedra at 14 GPa.

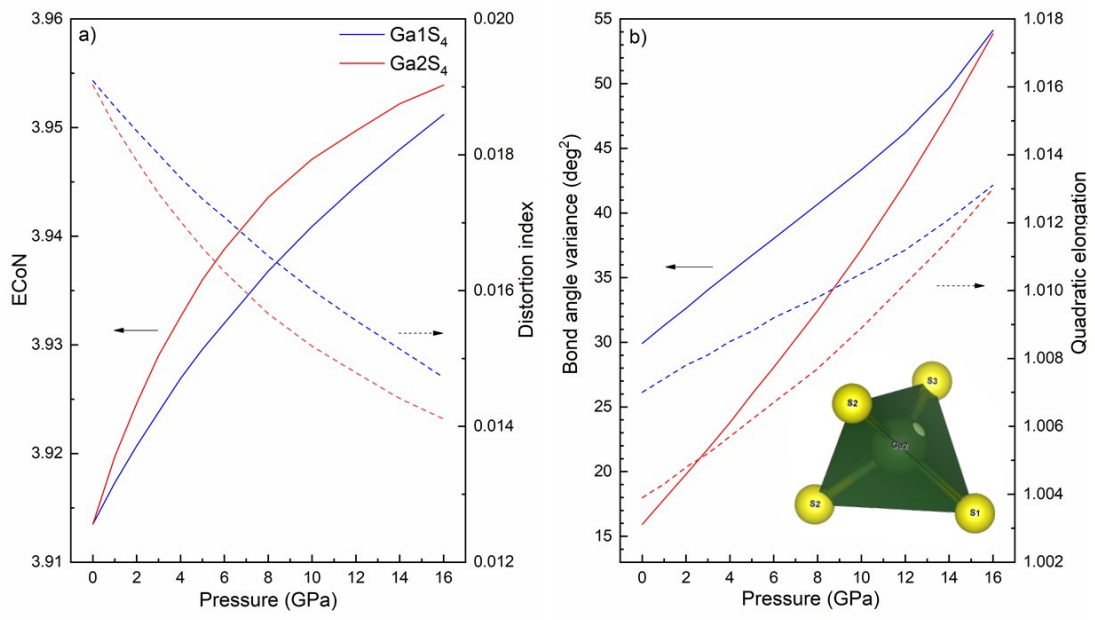

Figs. S5, S6 and **S7** show the relative change of the free theoretical atomic coordinates (x,y,z) of the unequivalent Ga and S atoms at HP. In general, it can be inferred that S atoms move more than Ga atoms at HP. However, we must highlight the particular features observed in each figure. As **Fig. S5 a)** shows, S1 and S2 atoms displace along the positive *a* axis while S3 atoms move in the opposite direction (**Fig. S5 b)**). Moreover, the change of the atomic parameters of the S3 atom is considerably larger than those of S1 and S2 atoms. These movements lead to the closing of the channels (see **Fig. S8 c)**). Concerning the Ga atoms, below ~4 GPa, Ga1 and Ga2 atoms move along the positive and negative *a* axis, respectively, which also leads to the closure of the channels (**Fig. S8 a)**). Above that pressure, Ga1 and Ga2 atoms start to move in the opposite direction as if there was some kind of repulsion along the *a* axis (**Fig. S5 a)**). Along the positive *b* axis, S atoms again move in a more pronounced way than Ga atoms (**Fig. S6**). Again around 4 GPa, Ga2 atoms change the movement direction from the positive to the negative *b* axis as if there were a repulsive effect above that pressure.

Figure S8 shows the displacement of S and Ga atoms in the *a*-*b* plane. Below ~4 GPa, Ga atoms move approximately symmetrically along the *b* axis (**Fig. S8 a)**). Above ~4 GPa they also move in a similar trend, where the axis of symmetry is now at around 60 degrees, measured to the *b* axis, from *a* to *b* (**Fig. S8 b)**). More surprising is how S and Ga atoms move along the z axis; i.e. along the direction normal to the *a*-*b* plane (**Fig. S7**). S1 and Ga1 atoms displace along the positive z cartesian axis, while S2 atoms move slightly in the opposite direction (**Fig. S7 a)**). In contrast, S3 atoms move along the positive z axis up to around 2 GPa and in the negative direction above that pressure. The most striking feature is that the relative z coordinate of the Ga2 atoms steadily decreases to 0 above 16 GPa (see **Fig. S7 b)**); i.e. it points to a symmetrisation of the structure that ends in the phase transition that has been observed above this pressure (see **Fig. 2**).

Figure S9 shows the displacements along the z cartesian axis of the S and Ga atoms. We have remarked that Ga1 and Ga2 atoms move in the opposite direction (**Fig. S9 a)**), bearing in mind that atom Ga2 changes its z coordinate much faster than atom Ga1, as already commented. **Figure S9 b)** and **Figure S9 c)** emphasize the change in the direction of movement of the S3 atom below and above 2 GPa, respectively. Therefore, the analysis of the atomic movements at HP shows a tendence of the monoclinic structure to a symmetrisation at HP.

Figure S5. Relative change of the theoretical *x* atomic coordinate of independent a) S1, S2, Ga1 and Ga2 atoms and b) S3 atoms of the α' phase on increasing pressure.

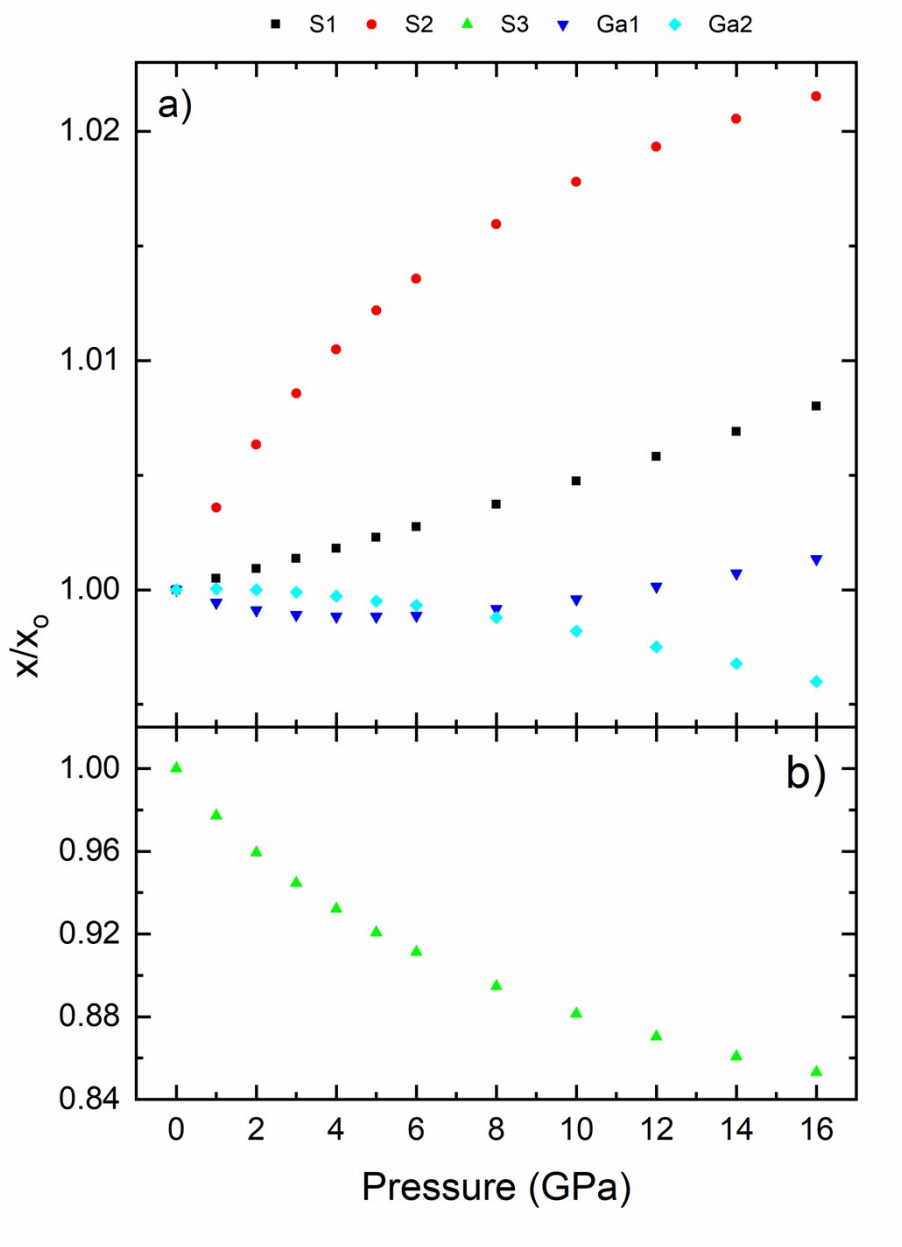

Figure S6. Relative change of the theoretical *y* atomic coordinate of all the independent atoms of the α' phase on increasing pressure.

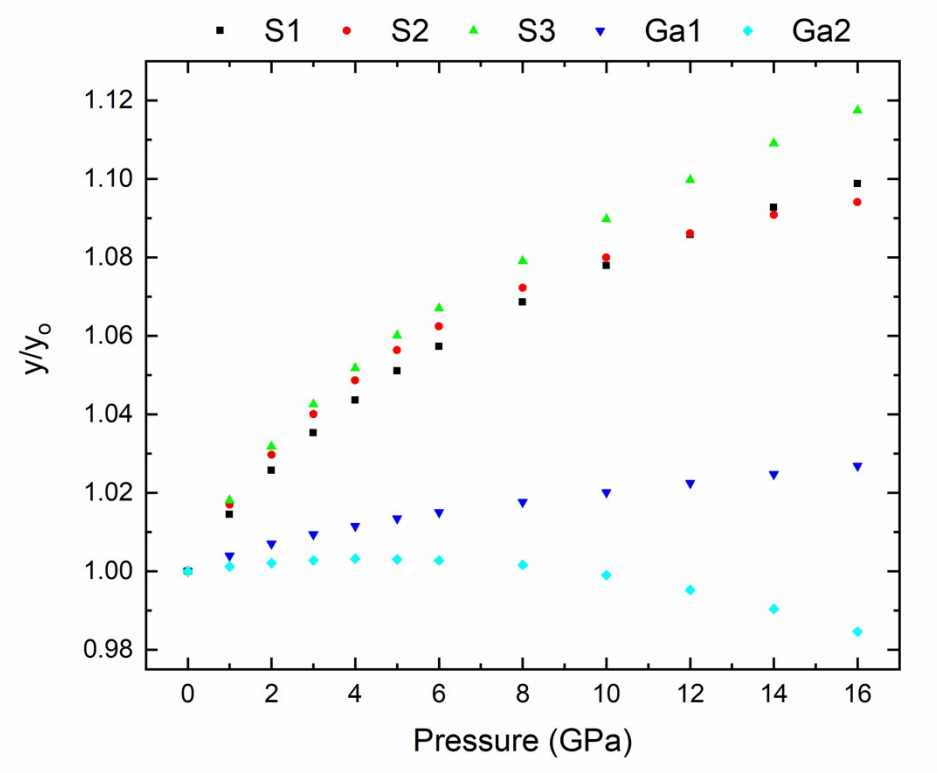

Figure S7. Relative change of the theoretical *z* atomic coordinate of independent a) S1, S2, S3 and Ga1 atoms and b) Ga2 atoms of the α' phase on increasing pressure.

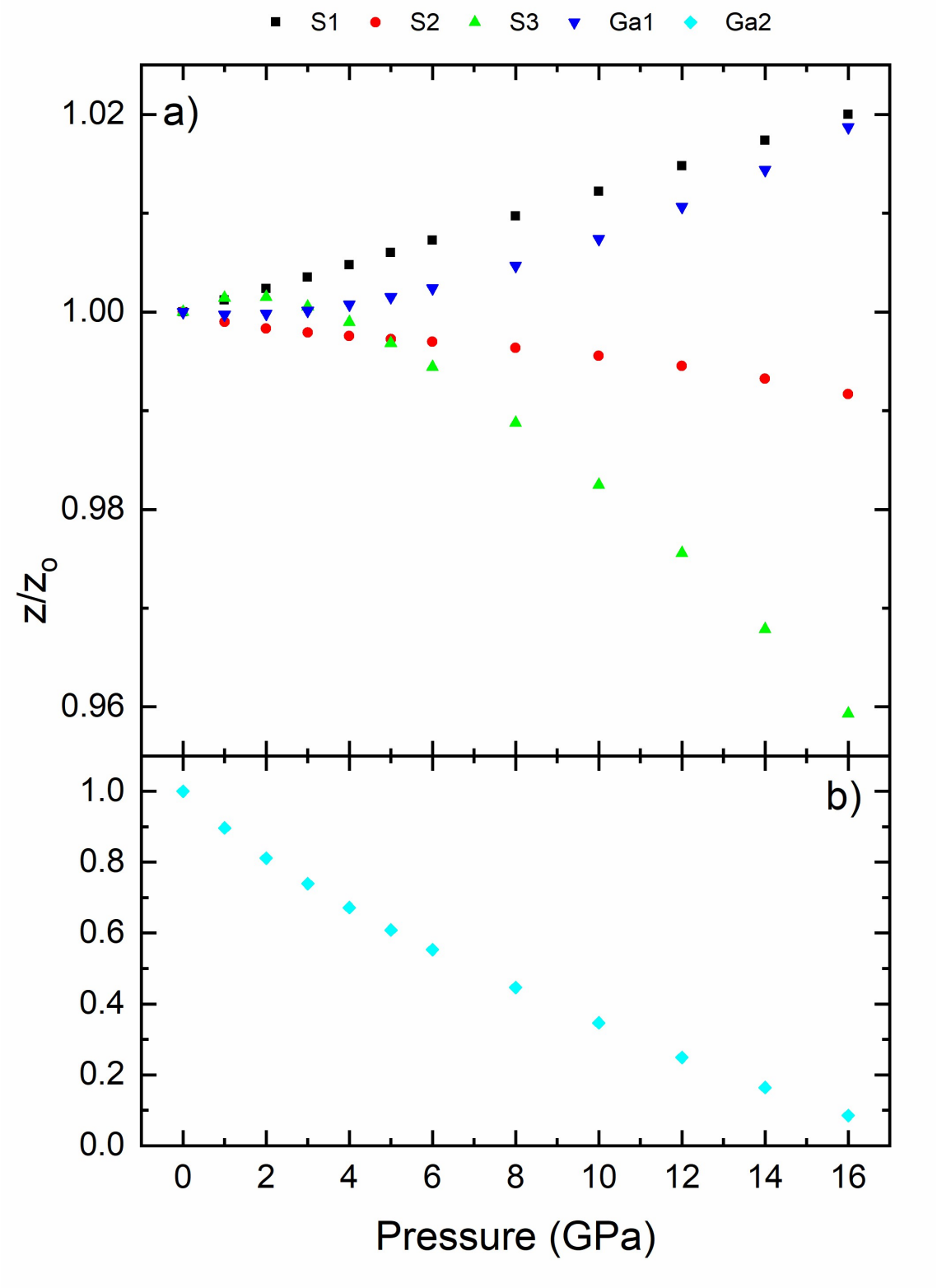

Figure S8. Schemes of the Ga_2S_3 structure around the vacancy. Arrows of each atom indicate the directions *x* and *y* of displacement of Ga atoms before a) and after 4 GPa b), and S atoms c) with increasing pressure. Dashed lines indicate the axis of symmetry about which the movement of Ga atoms is symmetrical. This axis is a) paralel to the *b* axis before 4 GPa and b) at around 60 degrees (measured to the *b* axis, from *a* to *b*) after 4 GPa.

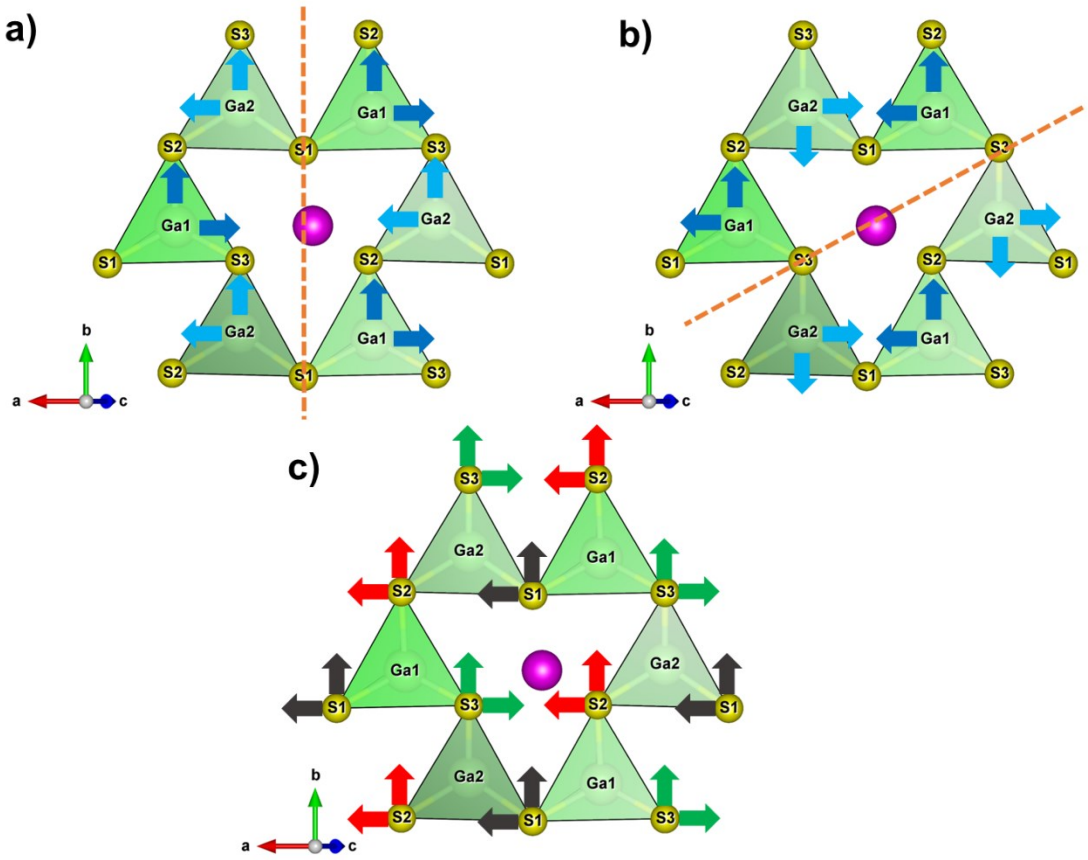

Figure S9. Schemes of α'-Ga_2S_3 around the vacancy. Arrows of each atom indicate the direction *z* of displacement of Ga atoms a) and S atoms b) before and c) after 2 GPa.

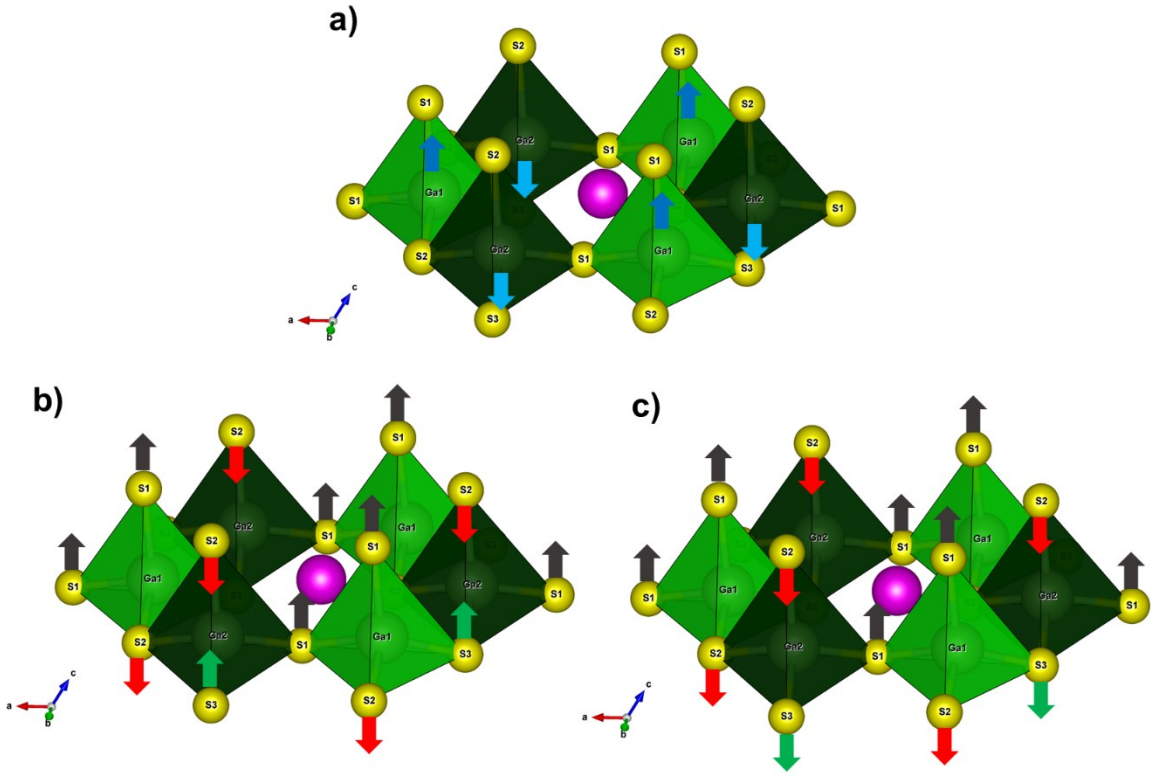

Vibrational properties

Figure S10. Scheme of the atomic vibrations of the *A'*(1) mode of α'-Ga_2S_3 around 74 cm^{-1}. This mode is a shear layer-like mode with all Ga and S atoms almost in the same plane of the wurtzite lattice vibrating out-of-phase with respect to all atoms of neighbour planes. It can be considered as a translation of the GaS_4 unit, despite it is a translation of the GaS_3 unit. Vibrations are observed thanks to software J-ICE.[2]

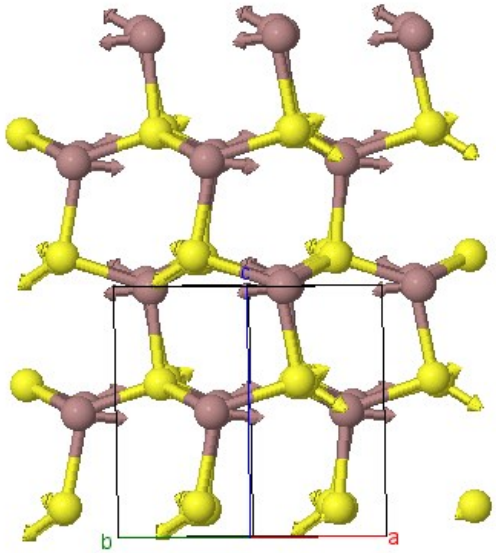

Figure S11. Scheme of the atomic vibrations of the *A''*(1) mode of α'-Ga_2S_3 around 82 cm^{-1}. This mode is also a shear layer-like mode with all Ga and S atoms almost in the same plane of the wurtzite lattice vibrating out-of-phase with respect to all atoms of neighbour planes. It can be considered as a translation of the GaS_4 unit, despite it is a translation of the GaS_3 unit. Note that this mode and the previous one are the two non-degenerate shear modes of typical shear E rigid modes of layered materials; i.e. atoms in both modes vibrate in perpendicular directions.

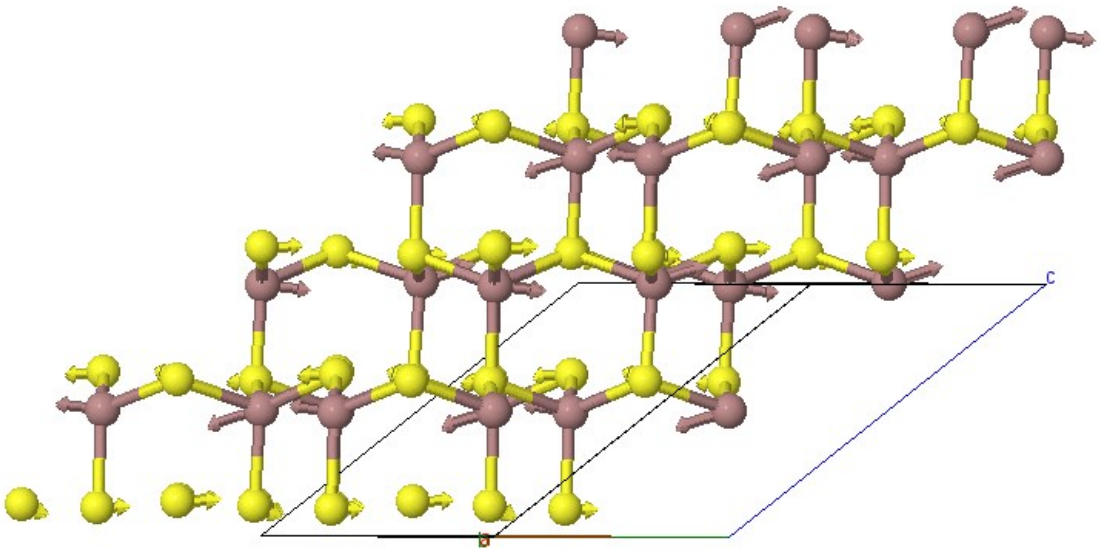

Figure S12. Scheme of the atomic vibrations of the *A'*(2) mode of α'-Ga_2S_3 around 87 cm^{-1}. This mode is mainly characterized by a strong movement of the S1 atom almost in perpendicular direction to the atomic planes of the wurtzite lattice. It also shows Ga1 atoms moving in opposite

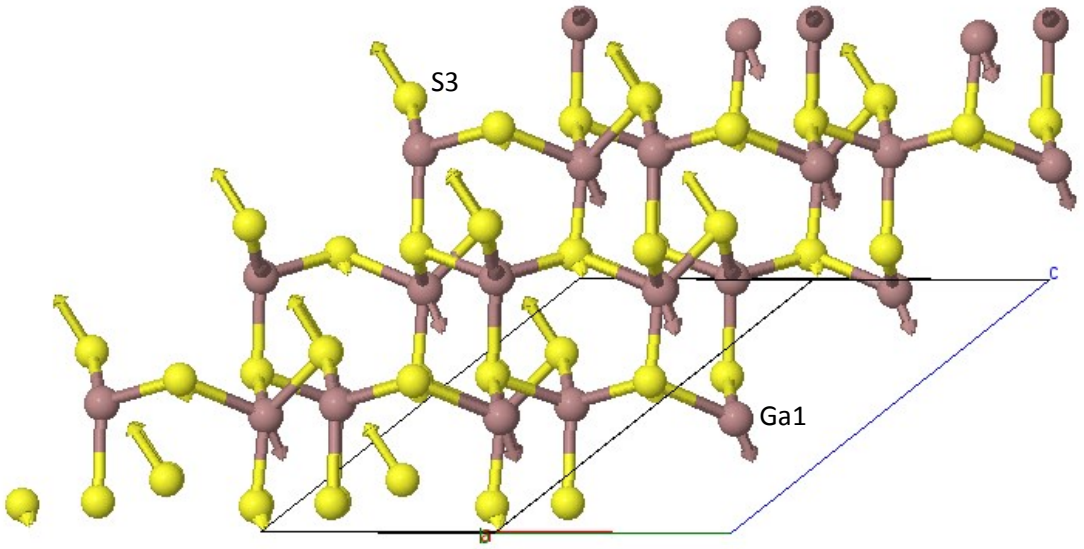

direction with respect to S3 atoms.

Figure S13. Scheme of the atomic vibrations of the *A''*(2) mode of α'-Ga_2S_3 around 100 cm^{-1}. This mode is a kind of compressional layer-like mode with all Ga and S atoms almost in the same plane of the wurtzite lattice vibrating out-of-phase with respect to all atoms of neighbour planes.

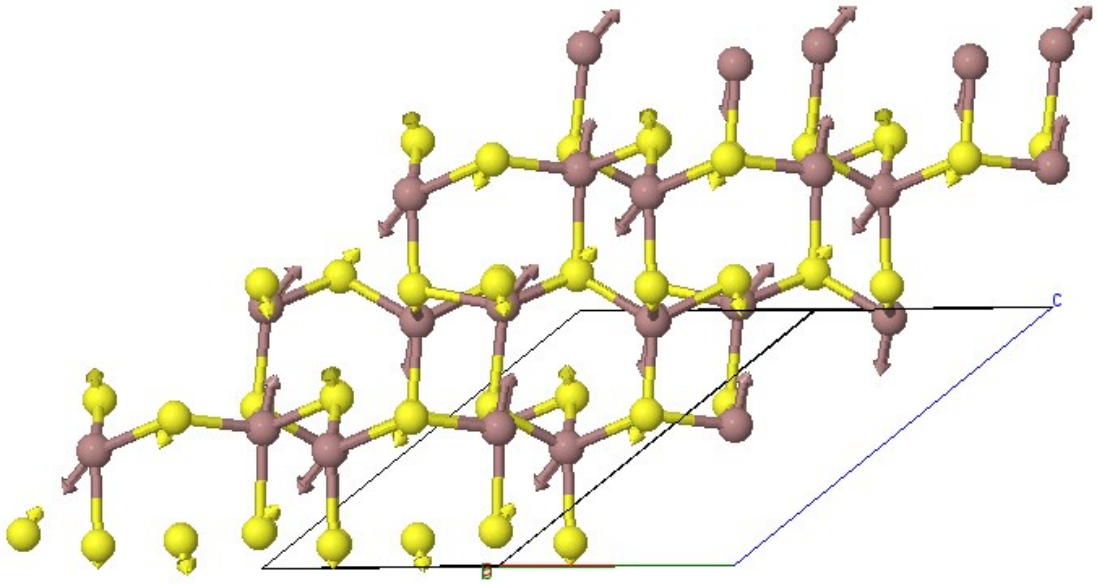

Figure S14. Scheme of the atomic vibrations of the *A'*(5) mode of α'-Ga_2S_3 around 147 cm^{-1}. This mode is a pure ν_4 bending mode of GaS_4 tetrahedra characterized by concerted movements of Ga and specially S3 atoms (that vibrate out-of-phase with respect to those of the neighbor layers).

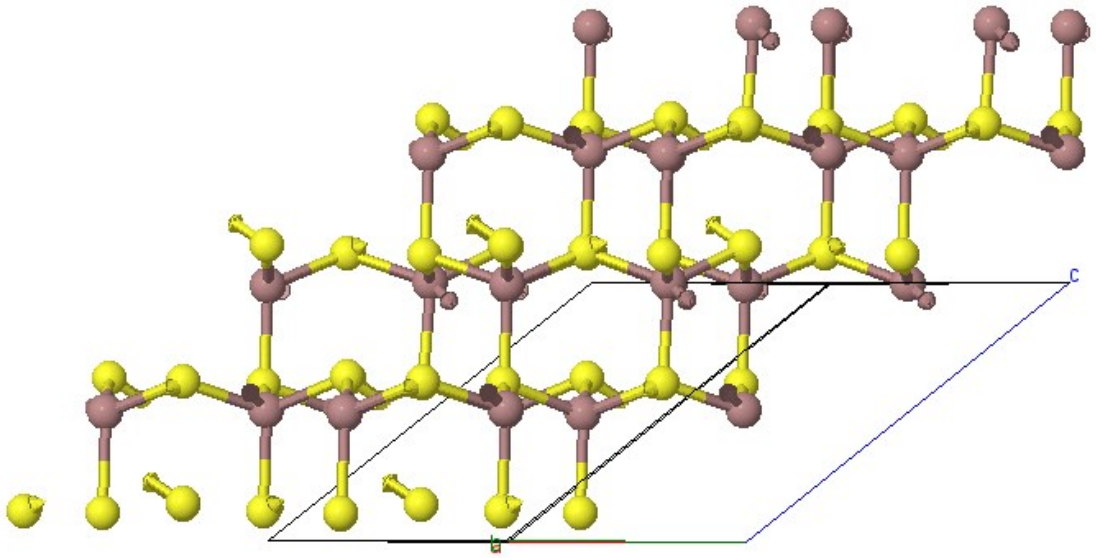

Figure S15. Scheme of the atomic vibrations of the *A'*(6) mode. The strongest Raman mode of α'-Ga_2S_3 around 234.6 cm^{-1}. This mode is a mixture of bending modes leaded by displacements of S1, S2 and S3 atoms. The concerted displacement of S atoms leads considerable symmetric stretching of S atoms around the vacancy and to a small symmetric Ga-S stretching ν_1 mode of the GaS_4 unit. This is why this mode is known also as the breathing mode of the vacancy. Note and S3 atom moves in the direction of the bisector of both cation vacancies around it (upward right in the figure), S2 atom vibrates against its neighbour vacancy (downward left in the figure),

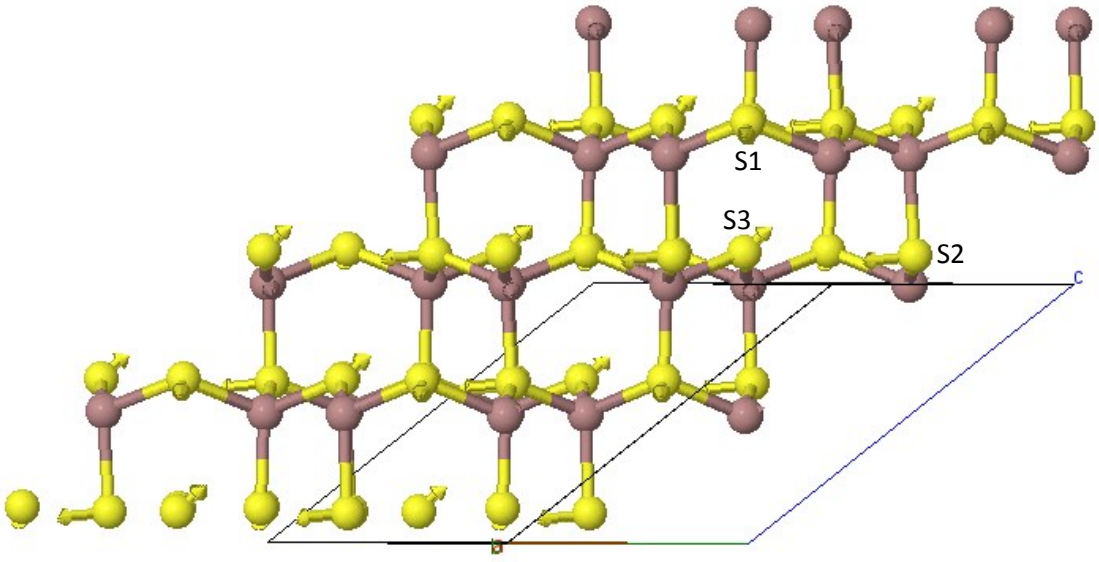

and S1 atom vibrates against its neighbour vacancy (downward front in the figure).

Figure S16. Scheme of the atomic vibrations of the *A'*(12) mode. The second strongest Raman mode of α'-Ga_2S_3 around 387 cm^{-1} is an asymmetric Ga-S stretching ν_3 vibration characterized mainly by S3 atomic vibrations (moving in-phase in the different layers) in the direction of the bisector of both cation vacancies around it (upward right in the figure), while Ga1 atoms (also moving in-phase in the different layers), but in opposite phase with respect to S3 atoms (downward left in the figure).

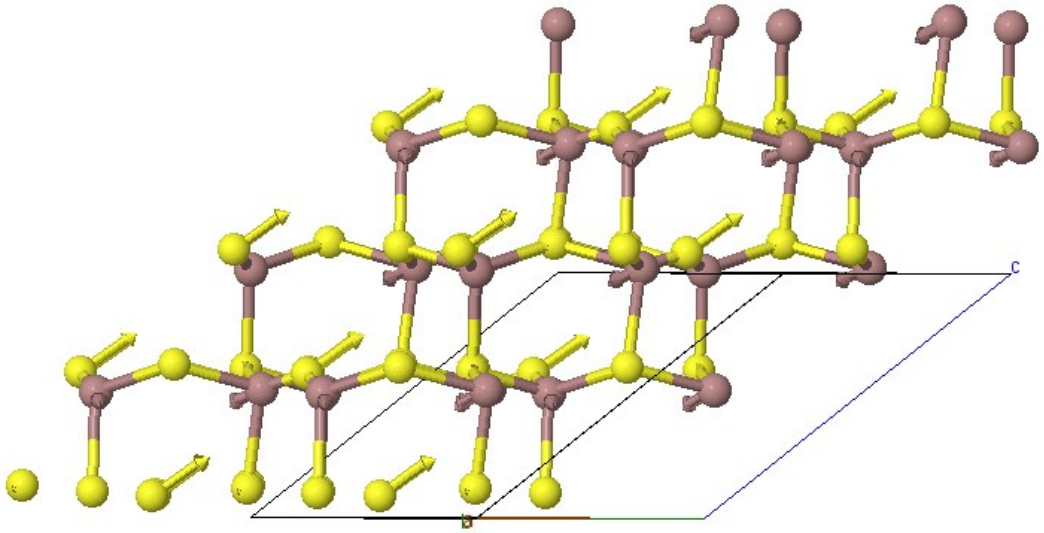

Figure S17. Scheme of the atomic vibrations of the *A''*(13) mode. This mode of α'-Ga_2S_3 around 392 cm^{-1} is an asymmetric Ga-S stretching ν_3 vibration characterized mainly by S3 atoms vibrations (moving out-of-phase in the different layers) in the direction of the bisector of both cation vacancies around it (upward right in the figure), while Ga1 atoms (also moving out-of-phase in the different layers), but in opposite phase with respect to S3 atoms (downward left in the figure).

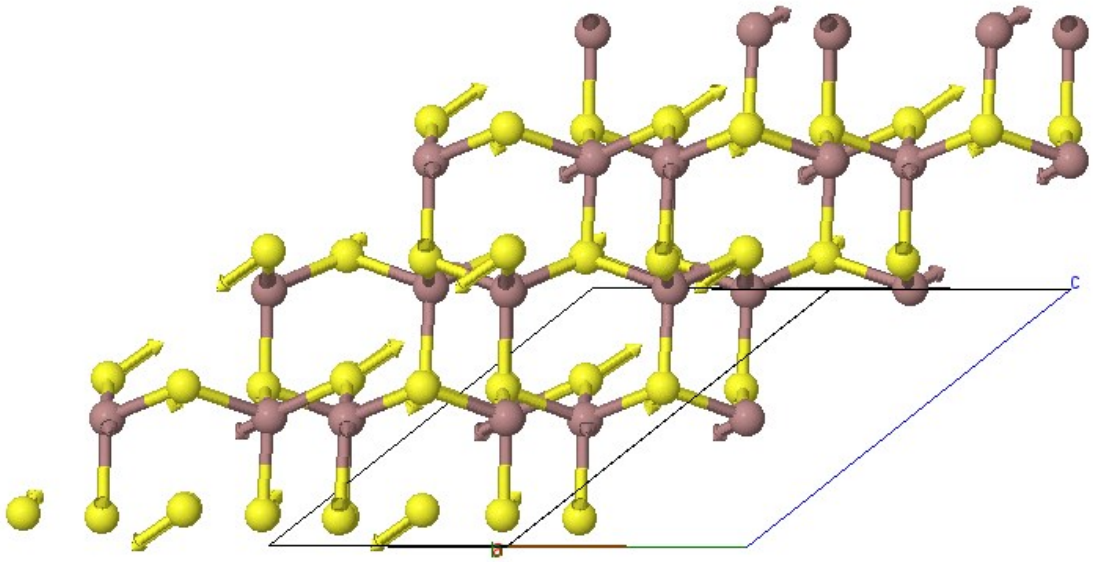

Figure S18. Scheme of the vibration of the *A''*(14) mode of α'-Ga_2S_3 around 407 cm^{-1}. This mode is an asymmetric Ga-S stretching ν_3 vibration characterized mainly by an in-phase movement of all S3 atoms in the direction of the two Ga atoms linking the S3 atom. View along the direction perpendicular to the wurtzite-like layers.

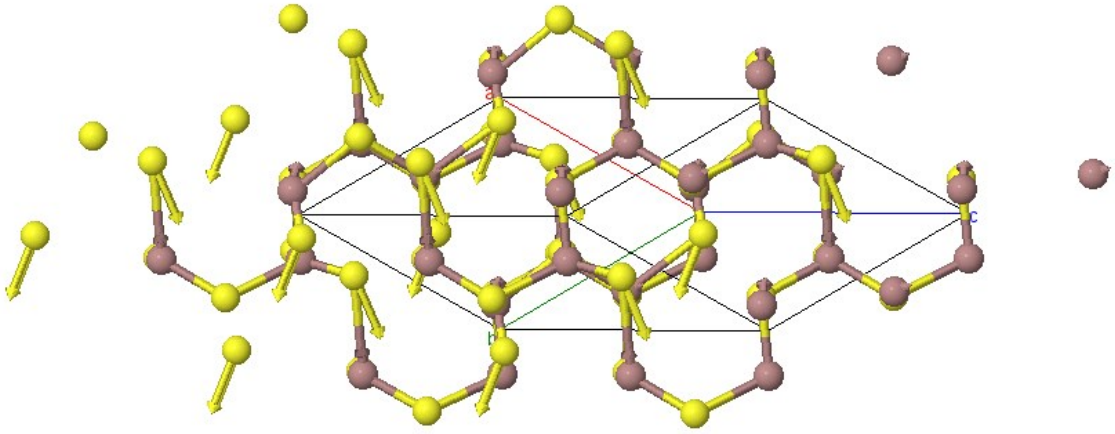

Figure S19. Scheme of the vibration of the *A'*(13) mode of α'-Ga_2S_3 around 425 cm^{-1}. This mode is an asymmetric Ga-S stretching ν_3 vibration characterized mainly by an out-of-phase movement of the closest S3 atoms in the direction of the two Ga atoms linking the S3 atom. View along the direction perpendicular to the wurtzite-like layers.

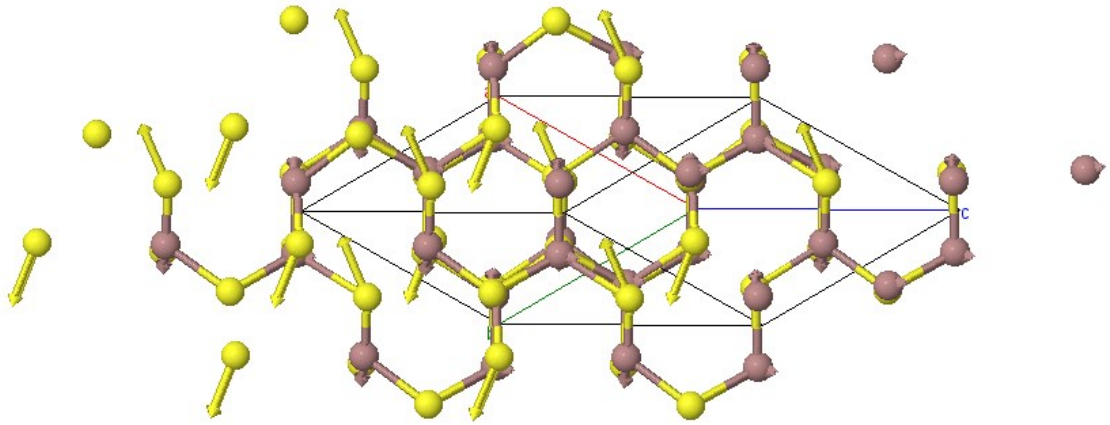

Figure S20. Theoretical one-phonon density of states of α'-Ga_2S_3 at 0 GPa. The total as well as the partial contribution of Ga and S atoms to the different vibrations is plotted. The individual contribution of the S atoms is also plotted in order to show the different contributions of S1, S1 and S3 atoms. Individual contribution of the Ga atoms is not plotted since both Ga1 and Ga2 atoms show similar contributions in all the regions.

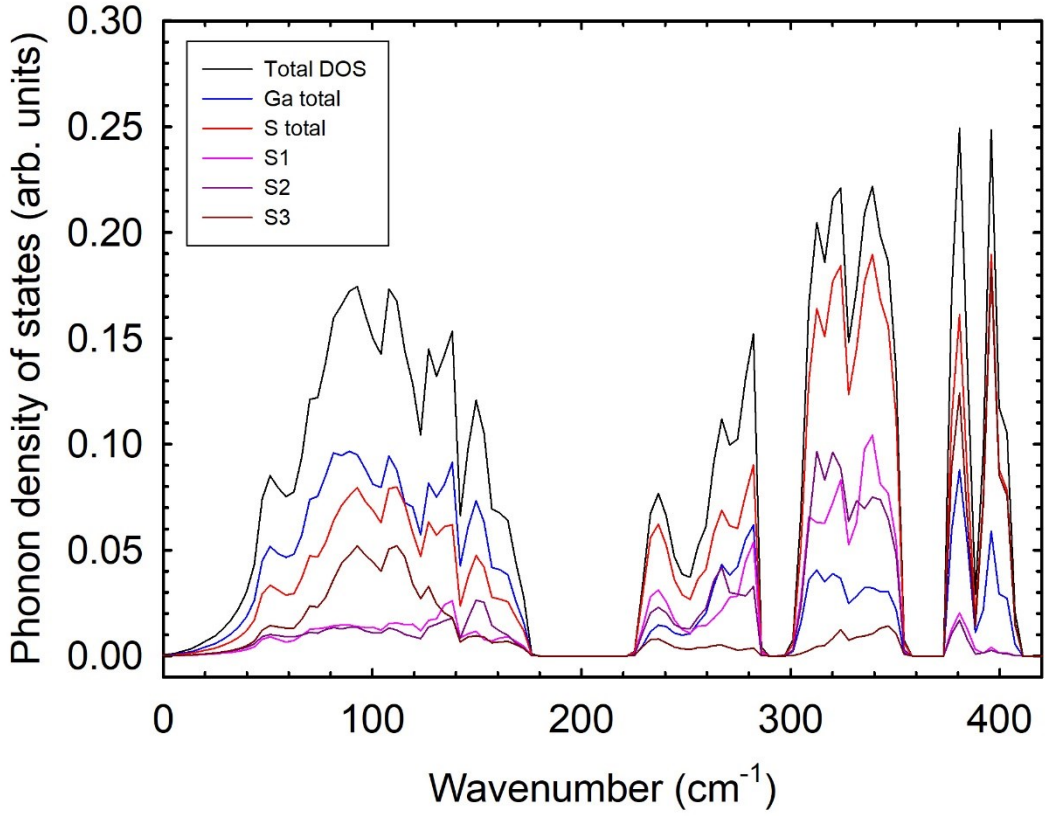

Figure S21 shows the normalized Raman spectra at 1048 and 1123 K. It can be seen that at these high temperatures all modes of α'-Ga_2S_3 have completely disappeared (see the comparison with the spectrum at 948 K in **Figure 8** of the main text). Moreover, two broad peaks emerge in the range from 500 to 800 cm^{-1}. These new peaks cannot be due to a temperature-induced phase transition of the α'-phase, because it melts congruently at about 1300 K.[3, 4] Therefore, we consider that these new peaks must come from the Ga_2O_3 impurity observed in our HP-XRD measurements. β-Ga_2O_3 exhibits 15 Raman-active optical modes $\Gamma = 10A_g + 5B_g$. Thanks to **Ref. 5** (see **Table 1**), we can confirm the presence of the β-Ga_2O_3 by assigning the symmetry of each mode observed in our Raman spectra, as can be seen in **Figure S21**. The ^{A}g modes are observed in the XX, YY, ZZ and XY directions and the ^{B}g modes in the YZ and XZ directions. For this reason, several modes cannot be seen properly in our unpolarised HT-RS measurements where several modes are overlapped. We have to notice that the Raman signals shown in **Fig. S21** are quite weak (RS spectra are shown with 50x factor in comparison with that of the α' phase) and that this observation is coherent with the small fraction of β-Ga_2O_3 in the original sample.

Figure S21. HT normalized Raman spectra of β-Ga_2O_3 at 1048 and 1123 K.

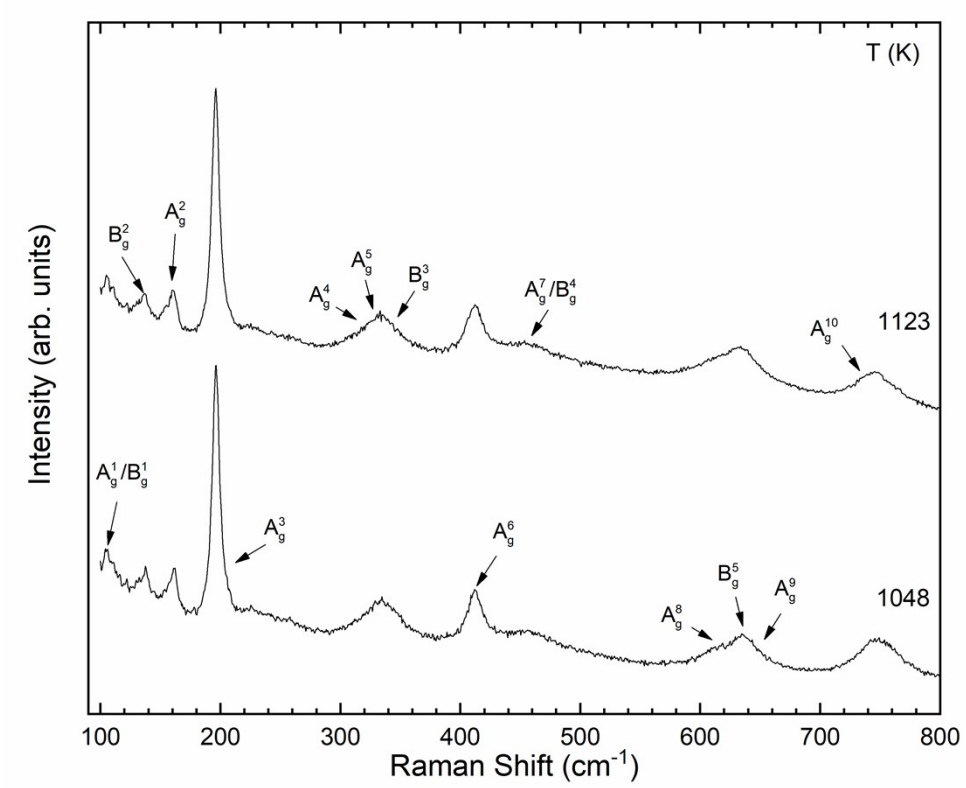

Figure S22. Temperature dependence of the experimental Raman-active mode frequencies of α'-Ga_2S_3.

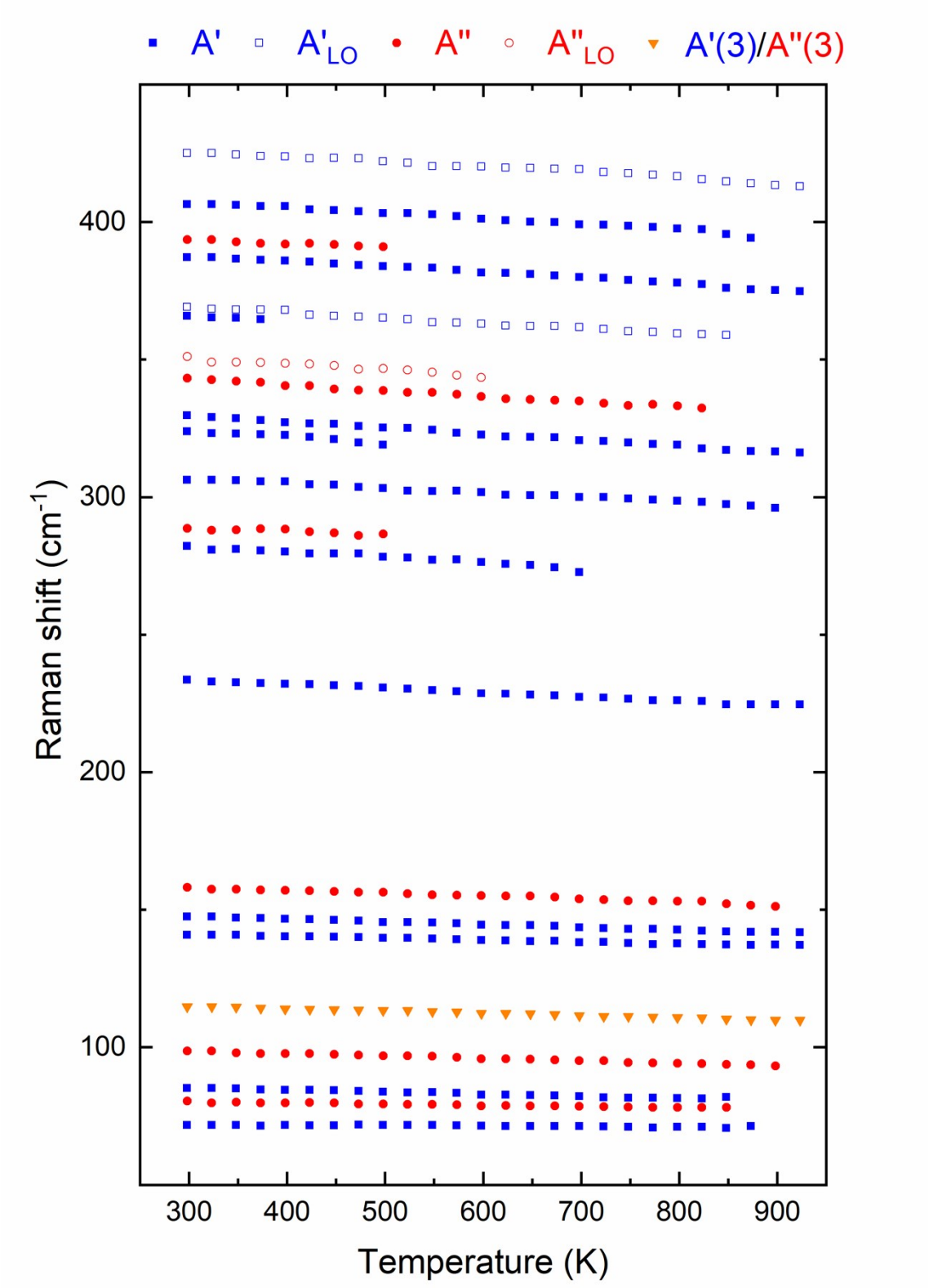

Figure S23. Temperature dependence of the FWHM of the *A'*(6) mode. Cubic, quartic and harmonic contributions are shown.

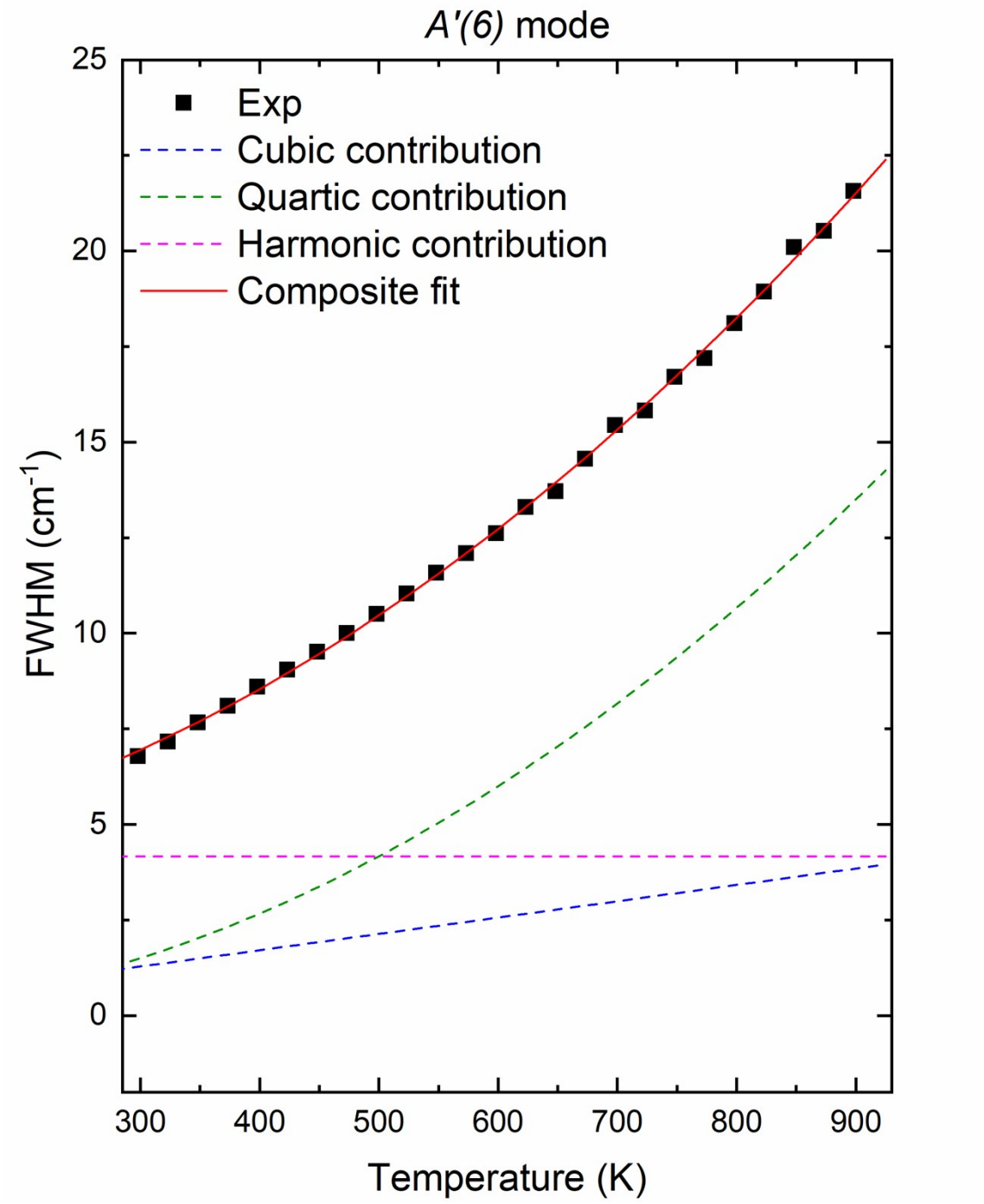

The isothermal mode Grüneisen parameter, γ_i^T, has been tabulated under the quasi-harmonic approximation according to the following equation:[6]

$$\gamma_i^T = \left(B_0/\omega_i\right)\left(d\omega_i/dP\right) \tag{1}$$

where ω_i and B_0 are the frequency of each mode and the isothermal bulk modulus, respectively. On the other hand, the isothermal averaged Grüneisen parameter from the macroscopic definition, γ_{av}^T, is defined as:[7]

$$\gamma_{av}^T = 3\alpha V_m B_0/C_v \tag{2}$$

expressed in terms of thermal expansion coefficient, α, molar volume, V_m, and molar heat capacity, C_v. From the microscopic definition, γ_{av}^T can be obtained as:

$$\gamma_{av}^T = \sum C_i\gamma_i/C_v \tag{3}$$

where C_i corresponds to the Einstein molar heat capacity and C_v is defined as $C_v = \sum C_i$. In particular, C_i is obtained as a function of the energy of each mode, $E_i = hv_i$, as:

$$C_i = R\frac{\left(E_i/k_BT\right)^2 e^{E_i/k_BT}}{\left(e^{E_i/k_BT} - 1\right)^2} \tag{4}$$

where v_i is the frequency in Hz, *T* the temperature, and k_B, h and *R* are the Boltzmann, Planck and ideal gas constants, respectively.

The simplest model proposed by Klemens allows us to qualitatively describe the mode frequency shift at HT as a function of the phonon-phonon coupling as follows:[8-10]

$$\omega_i = \omega_{io} + A\left[1 + \frac{2}{e^x - 1}\right] + B\left[1 + \frac{3}{e^y - 1} + \frac{3}{\left(e^y - 1\right)^2}\right] \tag{5}$$

where A and B are the cubic and quartic anharmonic contributions; i.e., decays of one phonon through third- and fourth-order processes into two or three modes of frequency $\omega_o/2$ or $\omega_o/3$, respectively, and where the exponents refer to $x = \hbar\omega_o/2k_BT$ and $y = \hbar\omega_o/3k_BT$, being ħ the reduced Planck's constant. It has to be said that **Eq. 5** has another term in the right side, which takes into account the mode shift at HT due to the thermal expansion of the lattice.[11-13] We do not have HT-XRD measurements to obtain the temperature dependence of the thermal expansion to consider this missing term. However, this is an approach to get knowledge of the third- and fourth-order processes that govern the temperature dependence of the modes.[8, 9]

The FWHM varies at HT due to the phonon-phonon coupling according the equation:[8]

$$\Gamma_i = \Gamma_{io} + C\left[1 + \frac{2}{e^x - 1}\right] + D\left[1 + \frac{3}{e^y - 1} + \frac{3}{\left(e^y - 1\right)^2}\right] \tag{6}$$

where C and D are the cubic and quartic anharmonic contributions, respectively.

Under the assumption of the quasiharmonic approximation, the mode frequency shifts observed at HP are the result of the variation of bond distances and thus their force constants. However, such an assumption is not fulfilled at HT since the mode frequency shifts observed in RS spectra depend on two effects: the volume (implicit) effect caused by the lattice thermal expansion and the temperature (explicit) effect related to phonon-phonon coupling.[14-16] These two contributions can be decoupled thanks to HP-RS and HT-RS measurements as follows:

$$\left(\frac{d\omega_i}{dT}\right)_P = -\frac{\alpha}{\beta}\left(\frac{d\omega_i}{dP}\right)_T + \left(\frac{d\omega_i}{dT}\right)_V \quad (7)$$

where β is the volume compressibility. The left-hand side of the **Eq. 7** is the isobaric temperature derivative of the mode frequency; that is, the total effect of the temperature on the mode shift, obtained from our HT-RS measurements. The first term in the right-hand side is the isothermal pressure derivative of the mode frequency, the implicit effect, obtained from our HP-RS measurements. The second term is the isochoric temperature derivative of the mode frequency; i.e. the explicit effect. We can reformulate the **Eq. 7** in terms of the mode Grüneisen parameters: [13, 17]

$$\gamma_i^P = \gamma_i^T + \gamma_i^V \quad (8)$$

where the isobaric and isochoric mode Grüneisen parameters are $\gamma_i^P = \left(-1/\alpha\omega_i\right)\left(d\omega_i/dT\right)_P$ and $\gamma_i^V = \left(-1/\alpha\omega_i\right)\left(d\omega_i/dT\right)_V$, respectively.[13, 14] Therefore, we can evaluate the relevance of the explicit effect, γ_i^V, for each mode with **Eq. 8**. From **Eq. 2**, we have obtained the experimental α = $1.03 \cdot 10^{-5}$ K^{-1}, required to calculate γ_i^P.

The implicit fraction, η_i is given by: [18]

$$\eta_i = \frac{\alpha\left(d\omega_i/dP\right)_T}{\beta\left(d\omega_i/dT\right)_P} = \frac{\gamma_i^T}{\gamma_i^P} \quad (9)$$

Table S1. Zero-pressure theoretical (only TO) and experimetal frequencies, pressure coefficients, and isothermal mode Grüneisen parameter of the Raman-active modes of the α' phase. The evolution of the mode frequencies as a function of pressure has been fitted to $\omega_i = \omega_{io} + a_1 P + a_2 P^2$. For comparison, zero-pressure frequencies corresponding to Raman and IR experiments from **Ref. 19** are also shown.

	Theoretical				Experimental			
Mode	ω_0 (cm^{-1})	a_1 ($cm^{-1}\cdot GPa^{-1}$)	a_2 (10^{-2} $cm^{-1}\cdot GPa^{-2}$)	γ_i^T	ω_0 (cm^{-1})	a_1 ($cm^{-1}\cdot GPa^{-1}$)	a_2 (10^{-2} $cm^{-1}\cdot GPa^{-2}$)	γ_i^T
A'(1)	68.7	-0.3	-1.4	-0.2	74, 72[a]	-0.5	-0.9	-0.3
A''(1)	78.1	-0.2	-1.1	-0.1	82, 80[a]	-0.1	-1.0	-0.1
A'(2)	81.5	0.5	2.0	0.2	87, 86[a]	0.4	2.1	0.2
A''(2)	96.2	0.4	-0.4	0.2	100, 93(TO)[b], 98(LO)[a]	0.3	-0.4	0.2
A''(3)	110.0	1.7	-5.0	0.6	118, 115[b]	1.3	-2.0	0.5
A'(3)	111.3	0.6	-3.2	0.2	116, 114(TO)[a], 116(LO)[a]	0.6	-1.8	0.2
A'(4)	135.7	0.5	-0.7	0.2	143, 141[a]	0.7	-1.1	0.2
A'(5)	140.2	1.6	-5.4	0.4	147(TO), 146[a]	1.4	-3.0	0.5
					150(LO), 147[a]	2.0	-7.4	0.6
A''(4)	145.7	0.8	-0.8	0.2	148[b]			
A''(5)	151.8	0.7	2.4	0.2	159	0.8	1.2	0.2
A''(6)	168.6	2.8	-4.7	0.6	177, 172[b]	2.7	-3.5	0.7
A'(6)	229.3	7.7	-14.9	1.3	235, 233[a]	8.0	-17.5	1.6
A''(7)	263.6	6.3	-11.4	0.9	280[a]			
A'(7)	277.2	5.0	-7.0	0.7	283, 284[b]	5.5	-9.1	0.9
A''(8)	285.3	6.0	-11.3	0.8	290, 300[b]	6.3	-14.2	1.0
A'(8)	298.4	4.6	-7.2	0.6	307(TO), 307[a]	4.3	-3.7	0.7
					310(LO)	4.1	-3.8	0.6
A''(9)	313.5	3.6	-0.8	0.4	326[b]			
A'(9)	318.4	4.8	-8.9	0.6	324, 321[a]	5.2	-12.6	0.7
A'(10)	322.0	5.4	-10.5	0.6	331, 329[a]	5.4	-12.0	0.8
A''(10)	323.5	5.4	-9.4	0.6	335[b]			
A''(11)	336.5	3.4	-1.8	0.4	344(TO), 343[b]	4.2	-8.7	0.6
					351(LO), 355[b]	4.1	-8.3	0.5
A'(11)	337.8	3.2	0.2	0.4	366(TO), 368[a]	3.1	2.0	0.4
					372(LO)	3.9	-3.5	0.5
A''(12)	338.2	6.6	-10.9	0.7	364[b]			
A''(13)	378.5	4.8	-7.6	0.5	393, 390[b]	4.9	-7.1	0.6
A'(12)	379.3	4.8	-7.8	0.5	388, 386[a]	5.4	-10.4	0.7
A''(14)	391.4	3.3	-0.5	0.3	411(TO)[b]			
					417(LO)[b]			
A'(13)	391.6	3.6	0.3	0.3	407(TO), 404[a]	3.2	-0.3	0.4
					425(LO)	2.8	-0.3	0.3

[a] Raman modes according to Lucazeau and Leroy (**Ref. 19**).

[b] The same for IR modes.

Table S2. Room-temperature experimental frequencies and temperature coefficients, as obtained from our HT-RS measurements, where mode frequencies have been fitted to $\omega_i = \omega_{io} + b_1 T + b_2 T^2$. Experimental cubic and quartic anharmonic contributions and their absolute ratio are appened. Experimental isobaric, isothermal and isochoric mode Grüneisen parameters are also shown as estimations of the total, implicit and explicit effects. The related implicit fraction, η_i, is included.

Mode	ω_0 (cm^{-1})	b_1 (10^{-2} $cm^{-1}\cdot K^{-1}$)	b_2 (10^{-5} $cm^{-1}\cdot K^{-2}$)	A (cm^{-1})	B (10^{-3} cm^{-1})	|A/B| (10^3)	γ_i^P	γ_i^T	γ_i^V	η_i
A′(1)	72	0.1	-0.2	0.01	-0.02	0.38	0.4	-0.3	0.7	-0.77
A″(1)	80	-0.6	0.1	-0.05	0.02	3.17	5.9	-0.1	5.9	-0.01
A′(2)	85	-1.0	0.2	-0.10	0.03	3.17	9.8	0.2	9.6	0.02
A″(2)	99	-0.7	-0.1	-0.09	-0.02	3.63	8.1	0.2	7.9	0.02
A″(3)*	115	-0.7	-0.1	-0.09	-0.03	2.79	6.4	0.5	5.9	0.08
A′(3)*	115	-0.7	-0.1	-0.09	-0.03	2.79	6.4	0.2	6.1	0.04
A′(4)	141	-0.8	0.1	-0.13	0.04	3.29	5.0	0.2	4.8	0.05
A′(5)	148	-1.1	0.1	-0.19	0.03	5.43	6.8	0.4	6.4	0.07
A″(4)										
A″(5)	158	-0.4	-0.6	-0.07	-0.28	0.24	4.4	0.2	4.2	0.05
A″(6)										
A′(6)	234	-1.6	0.1	-0.44	0.06	6.93	6.4	1.6	4.8	0.25
A″(7)										
A′(7)	282	0.7	-2.7	0.22	-4.21	0.05	3.3	0.9	2.4	0.28
A″(8)	288	3.2	-5.4	1.03	-8.51	0.12	0.2	1.0	-0.8	4.14
A′(8)	307	-1.5	-0.1	-0.54	-0.27	2.03	5.1	0.7	4.4	0.13
A″(9)										
A′(9)	324	6.4	-10.9	2.32	-21.01	0.11	0.4	0.7	-0.4	2.05
A′(10)	330	-2.3	0.1	-0.89	0.18	5.09	6.6	0.8	5.9	0.11
A″(10)										
A″(11)	343(TO)	-2.9	0.8	-1.19	1.97	0.61	7.0	0.6	6.4	0.08
	350(LO)	0.5	-2.9	0.19	-7.03	0.03	3.6	0.5	3.0	0.15
A′(11)	366(TO)	-6.7	7.6	-2.94	21.57	0.14	5.7	0.4	5.3	0.07
	369(LO)	-2.7	0.7	-1.19	2.04	0.58	6.1	0.5	5.6	0.08
A″(12)										
A″(13)	394	-2.6	1.6	-1.19	5.07	0.23	4.0	0.6	3.4	0.15
A′(12)	387	-1.0	-0.9	-0.45	-2.54	0.18	3.8	0.6	3.1	0.17
A″(14)										
A′(13)	407(TO)	-0.9	-1.0	-0.42	-3.12	0.13	3.5	0.4	3.1	0.10
	425(LO)	-0.4	-1.2	-0.21	-4.34	0.05	2.6	0.3	2.3	0.12

Topological properties

The bulk modulus can be obtained from the different B_{oi} of each basin by the volume-weighted sum of the contributions as follows: [20]

$$\frac{1}{B_o} = \sum f_i \frac{1}{B_{oi}} \tag{10}$$

where $f_i = \frac{V_i}{V}$ is the fraction of the unit-cell volume occupied by the basin i.

The charge transfer is related with the Bader charges, Q_i, and the nominal oxidation states, OS_i, by means of the following relation:[21]

$$CT_i = \frac{Q_i}{OS_i} \tag{11}$$

Figure S24. Pressure dependence of a) atomic volumes, b) Bader atomic charges (Q_i) and c) charge transfers (CT_i) of the Ga and S basins.

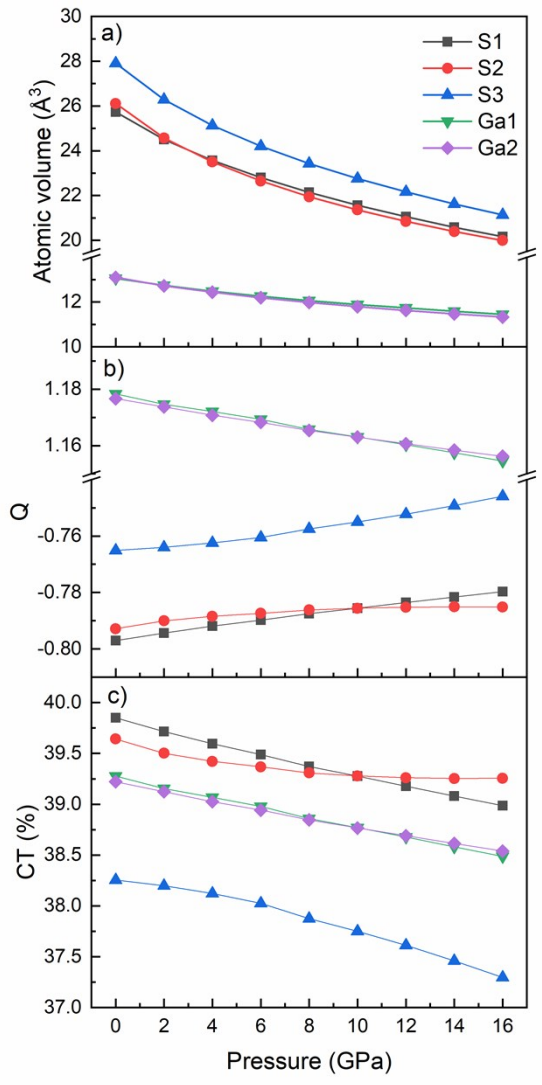

Figure S25. View of α'-Ga_2S_3 perpendicular to the *c*-axis with the bond critical points (BCPs). Orange and brown balls refer to Ga-S BCPs. The former is related with the S3 atoms and the latter with the S1 and S2 atoms. Red balls indicate the S1-S2 BCPs. The S1 and S2 atoms have also BCPs with the S3 atoms. They are represented with balls as follows: green (dark) balls refer to S1-S3(S3*) and violet (blue) refer to S2-S3(S3*), respectively. Asterisks indicate those atoms separated a longer distance. S-S BCPs are inside the channels, except the S3-S3 BCPs (gold balls) that are found between S3-S3 atoms.

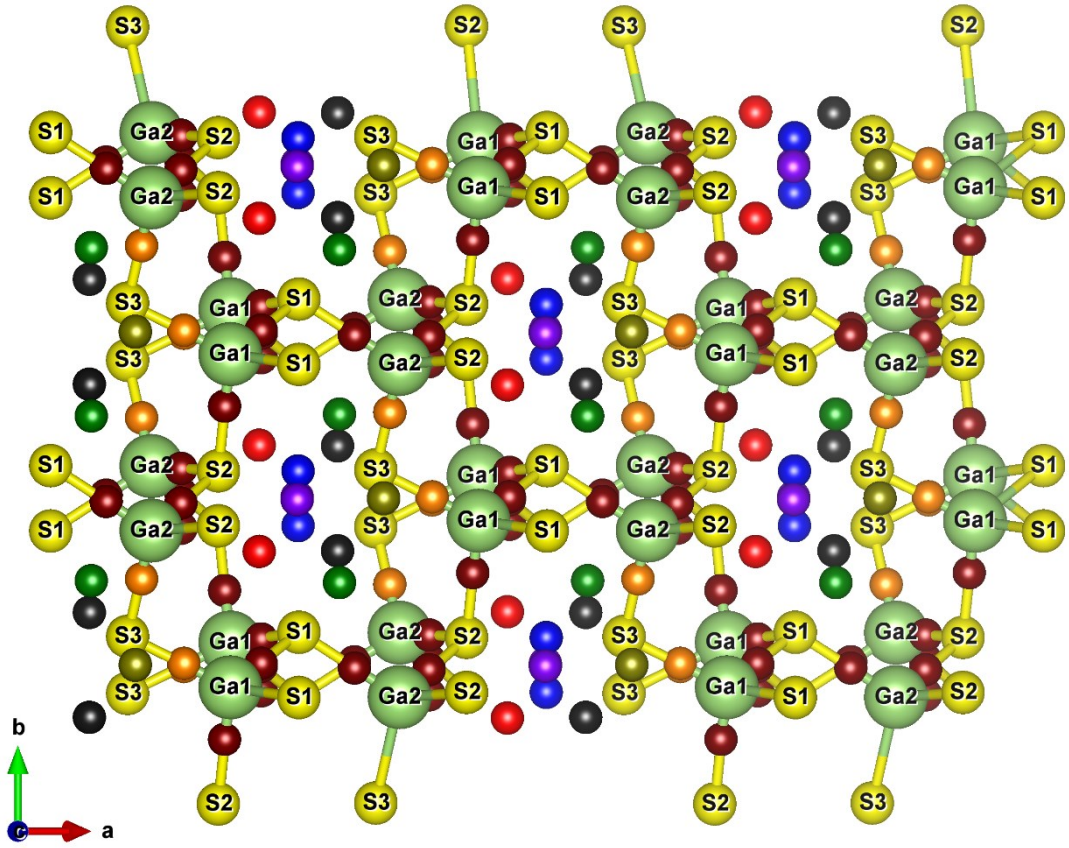

Figure S26. Theoretical all-electron 1D-ELF between Ga-S bonds for a) $Ga1S_4$ and b) $Ga2S_4$ tetrahedra at 0 GPa.

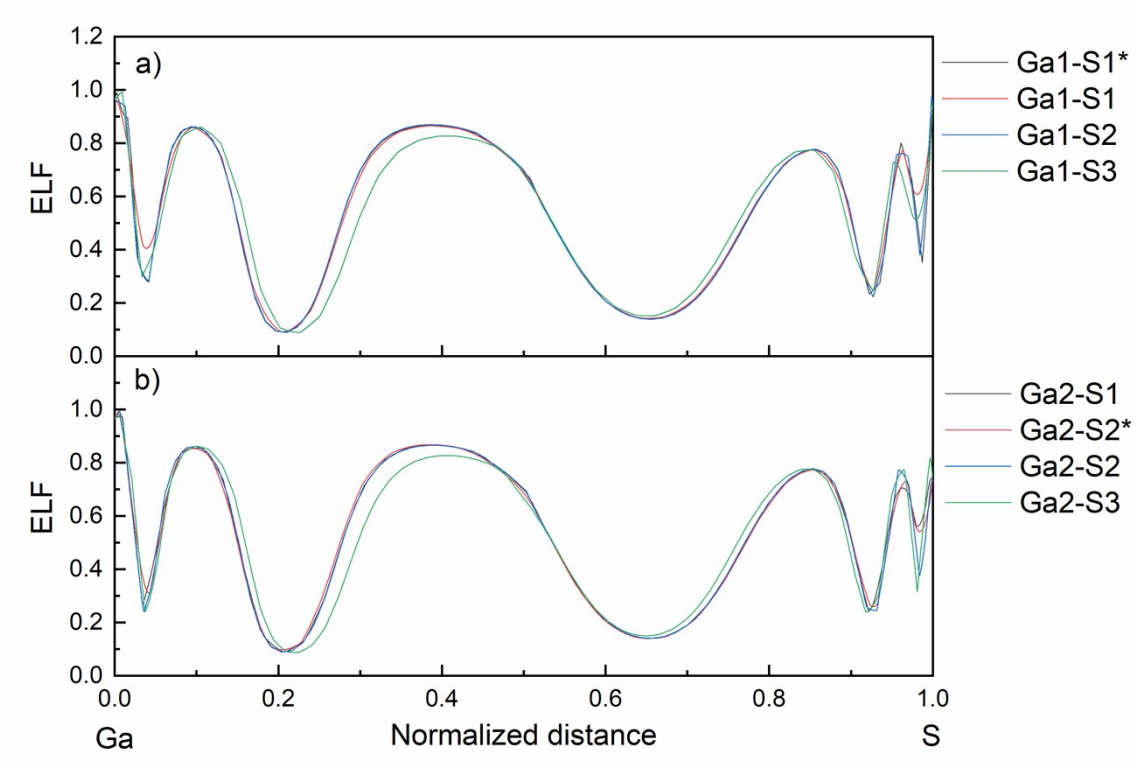

Electronic properties

Figure S27. The first Brillouin zone (BZ) and relevant high symmetry points of α'-Ga_2S_3.

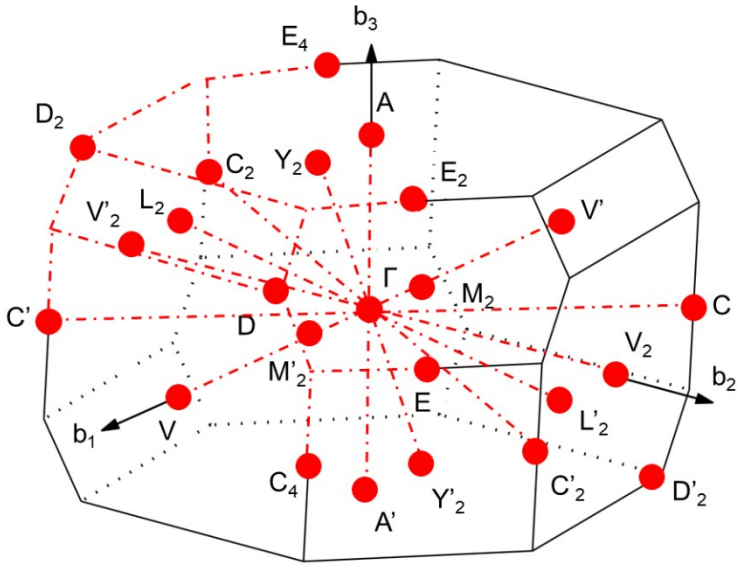

Figure S28. Atomic contributions to the electronic density of states (EDOS) of α'-Ga_2S_3 at different pressures: a) 0 GPa, b) 6 GPa, and c) 16 GPa.

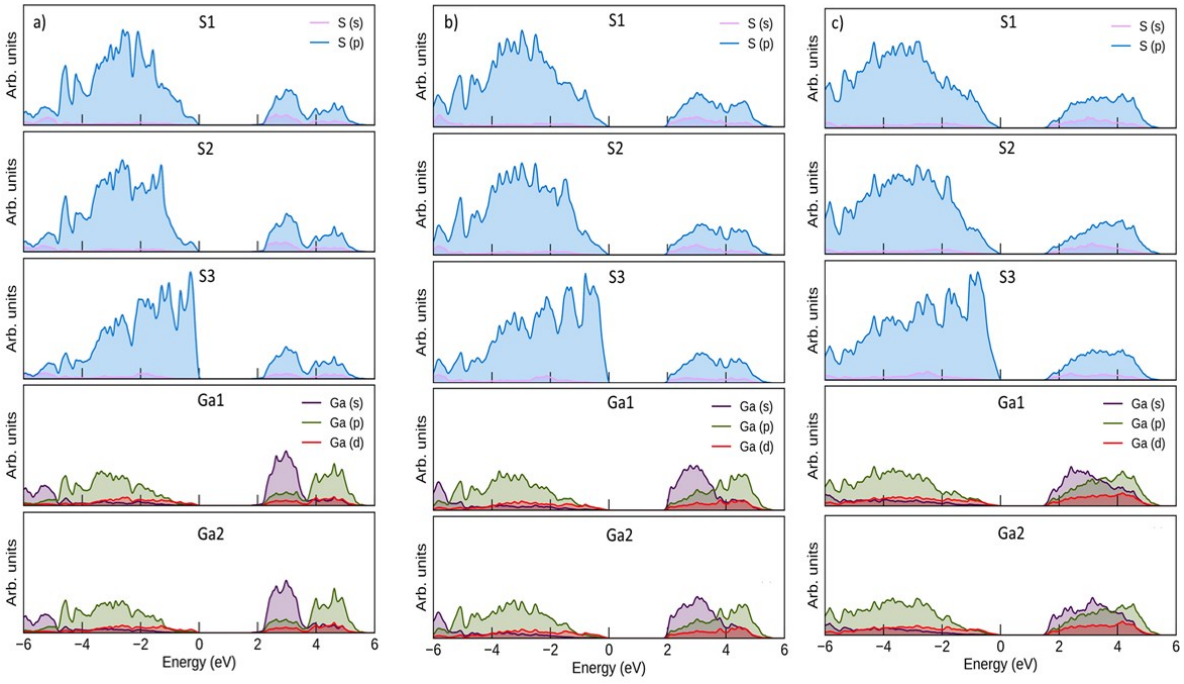

Figure S29. Electronic band structure and total and partial electronic density of states (EDOS) in α'-Ga_2S_3 at 6 GPa. The 1st valence band (VB) and the 1st and 2nd conduction bands (CB) are labelled.

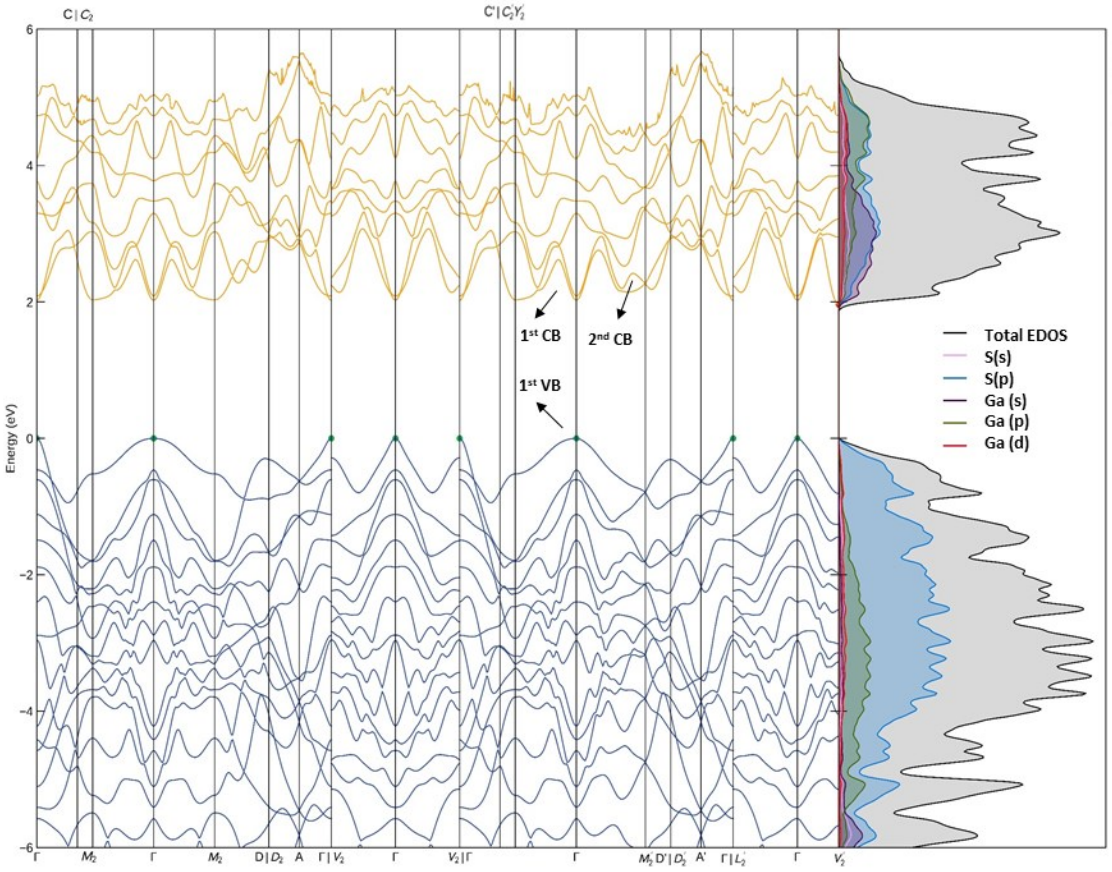

References

(1) Lai, X.; Zhu, F.; Qin, S.; Chen, D.; Li, Y.; Yang, K.; Wu, X. Experimental and theoretical identification of a high-pressure polymorph of Ga_2S_3 with α-Bi_2Te_3-type structure. *J. Appl. Phys.* **2014**, *116*, 193507.

(2) Canepa, P.; Hanson, R. M.; Ugliengo, P.; Alfredsson, M. J-ICE: a new Jmol interface for handling and visualizing crystallographic and electronic properties. *Journal of Applied Crystallography* **2011**, *44*, 225-229.

(3) Lieth, R.; Heijligers, H.; vd Heijden, C. The P-T-X Phase Diagram of the System Ga-S. *Journal of the Electrochemical Society* **1966**, *113*, 798-801.

(4) Pardo, M.; Guittard, M.; Chilouet, A.; Tomas, A. Diagramme de phases gallium-soufre et études structurales des phases solides. *J. Solid State Chem.* **1993**, *102*, 423-433.

(5) Onuma, T.; Fujioka, S.; Yamaguchi, T.; Itoh, Y.; Higashiwaki, M.; Sasaki, K.; Masui, T.; Honda, T. Polarized Raman spectra in β-Ga_2O_3 single crystals. *Journal of crystal growth* **2014**, *401*, 330-333.

(6) Grüneisen, E. Theorie des festen Zustandes einatomiger Elemente. *Annalen der Physik* **1912**, *344*, 257-306.

(7) Barron, T. H. K. Grüneisen parameters for the equation of state of solids. *Annals of Physics* **1957**, *1*, 77-90.

(8) Balkanski, M.; Wallis, R.; Haro, E. Anharmonic effects in light scattering due to optical phonons in silicon. *Physical Review B* **1983**, *28*, 1928.

(9) Sarantopoulou, E.; Raptis, C.; Ves, S.; Christofilos, D.; Kourouklis, G. Temperature and pressure dependence of Raman-active phonons of $CaMoO_4$: an anharmonicity study. *J. Phys.: Condens. Matter* **2002**, *14*, 8925.

(10) Bevara, S.; Mishra, K. K.; Patwe, S. J.; Ravindran, T.; Gupta, M. K.; Mittal, R.; Krishna, P. S. R.; Sinha, A. K.; Achary, S. N.; Tyagi, A. K. Phase transformation, vibrational and electronic properties of $K_2Ce(PO_4)_2$: a combined experimental and theoretical study. *Inorganic chemistry* **2017**, *56*, 3335-3348.

(11) Spanier, J. E.; Robinson, R. D.; Zhang, F.; Chan, S.-W.; Herman, I. P. Size-dependent properties of CeO_{2-y} nanoparticles as studied by Raman scattering. *Physical Review B* **2001**, *64*, 245407.

(12) Deshpande, M.; Bhatt, S. V.; Sathe, V.; Rao, R.; Chaki, S. Pressure and temperature dependence of Raman spectra and their anharmonic effects in Bi_2Se_3 single crystal. *Phys. B* **2014**, *433*, 72-78.

(13) Kourouklis, G.; Anastassakis, E. Pressure-induced phase transitions and anharmonicity study of alkaline-earth fluorides. *phys. status solidi (b)* **1989**, *152*, 89-99.

(14) Lucazeau, G. Effect of pressure and temperature on Raman spectra of solids: anharmonicity. *J. Raman Spectrosc.* **2003**, *34*, 478-496.

(15) Peercy, P.; Morosin, B. Pressure and Temperature Dependences of the Raman-Active Phonons in SnO_2. *Physical Review B* **1973**, *7*, 2779.

(16) Weinstein, B. A.; Zallen, R. In *Light Scattering in Solids IV*; Springer: 1984; pp 463-527.

(17) Bhatt, S. V.; Deshpande, M.; Sathe, V.; Rao, R.; Chaki, S. Raman spectroscopic investigations on transition-metal dichalcogenides MX_2 (M= Mo, W; X= S, Se) at high pressures and low temperature. *J. Raman Spectrosc.* **2014**, *45*, 971-979.

(18) Zallen, R.; Conwell, E. The effect of temperature on libron frequencies in molecular crystals: Implications for TTF-TCNQ. *Solid State Communications* **1979**, *31*, 557-561.

(19) Lucazeau, G.; Leroy, J. Etude vibrationnelle de α Ga_2S_3. *Spectrochimica Acta Part A: Molecular Spectroscopy* **1978**, *34*, 29-32.

(20) Pendás, A. M.; Costales, A.; Blanco, M.; Recio, J.; Luaña, V. Local compressibilities in crystals. *Physical Review B* **2000**, *62*, 13970.

(21) Mori-Sánchez, P.; Pendás, A. M.; Luaña, V. A classification of covalent, ionic, and metallic solids based on the electron density. *Journal of the American Chemical Society* **2002**, *124*, 14721-14723.